RSC Advances

PAPER

View Article Online
View Journal | View Issue

CrossMark click for updates

Cite this: *RSC Adv.*, 2016, **6**, 57000

Steam treatment of a hollow lithium phosphate catalyst: enhancing carbon deposition resistance and improving the catalytic performance of propylene oxide rearrangement†

Yanan Wang,[a] Zhishan Li,[a] Weihua Ma,*[a] Grace Kinunda,[b] Hongxia Qu[a] and Qin Zhong[a]

Received 13th April 2016
Accepted 27th May 2016

DOI: 10.1039/c6ra09559c

www.rsc.org/advances

Carbon deposition is a great problem for most solid acid and base catalysts applied in organic catalytic reactions. Basic lithium phosphate catalyst, when used for propylene oxide rearrangement, is also easily deactivated due to carbon deposition. In this paper, a green surface modification technique of steam treatment was employed to suppress carbon deposition on the basic lithium phosphate catalyst and to improve its catalytic performance. The results showed that the catalyst which was pre-treated with steam at 300 °C for 30 minutes exhibited excellent catalytic activity. Furthermore, the amount of carbon deposition was 15.1%, much lower than that of the untreated catalyst (21.5%). The steam treatment could increase the amount of hydroxyl and adjust the distribution of the acid and base sites. The decrease of the amount of Brønsted acid sites resulted in the reduction of carbon deposition. The enhancement of activity could be attributed to the increase of synergistic sites, and this could be due to an increase in the amount of Lewis acid sites and in the strength of the base sites.

Published on 27 May 2016. Downloaded by University of Dar es Salaam on 9/18/2018 10:19:08 AM.

1. Introduction

The rearrangement of epoxides is an important process because it provides a simple method to obtain valuable key compounds in organic and pharmaceutical synthesis.[1,2] A number of Lewis- and Brønsted-acid catalysts have been successfully used for the rearrangement of epoxides.[2–5] Different catalysts lead to different products depending on the surface acid–base characteristics of the catalytic system.[6] Lewis acids, such as Pd(0)/PR_3,[7,8] Bi(OTf)$_3$·$x$$H_2O$,[9] $IrCl_3 \cdot xH_2O$[10] and Er(OTf)$_3$,[11] are useful to obtain ketones from epoxide rearrangements. Chromium(III) tetraphenylporphyrin triflate (CrTPP(OTf))[12] and chromium(III) phthalocyanine triflate (CrTBPC(OTf))[13] give the corresponding aldehydes from epoxides in a stereoselective manner. Asymmetric rearrangements of achiral epoxides to enantiomerically enriched allyl alcohols by the action of chiral lithium bases have emerged as one of the most useful methodologies in the field of asymmetric synthesis.[14,15]

For the rearrangement of propylene oxide, different catalysts may also result in different products, such as allyl alcohol, propionaldehyde, and acetone. The acid–base characteristics of the catalyst are important for the reaction. Some researchers have put forward that acid or base sites have an effect on the distribution of the reaction products. Acetone is prone to be produced on the base sites, while strong acid sites are beneficial to afford propionaldehyde. The production of allyl alcohol requires acidic and basic active sites.[16–18] Therefore, a wide range of catalysts which are applied to this rearrangement have attracted great attention.[9]

For the arrangement of most epoxides, the reactions take place in the liquid phase or the liquid–solid phase. For propylene oxide, however, there are two processes: the gas–solid phase and the slurry phase. The gas–solid phase process is much simpler and cleaner than the slurry phase; however, carbon deposition has always been a major problem. Therefore, it is important to suppress carbon deposition on the catalysts.[19] Coke formation is closely related to the nature and distribution of the acid sites.[20,21] Thus, many investigations have aimed at solving this problem *via* adjusting and controlling the distribution of the acid and base sites. It has been reported that steam treatment could decrease the coking rate and enhance the catalytic activity. Hongxia Wang *et al.*[22] revealed that post-steam-treatment could improve the catalytic performance of Mo/HZSM-5 catalysts in methane dehydroaromatization under nonoxidative conditions. Also, further studies on this catalyst led to the conclusion that the amount of free Brønsted acid sites per unit cell decreased after the steam treatment and also gave higher methane conversion and a higher yield of light aromatics, as well as a decrease in the rate of carbon deposition.

[a]*School of Chemical Engineering, Nanjing University of Science and Technology, Nanjing 210094, Jiangsu, People's Republic of China. E-mail: maweihuacn@163.com; Fax: +86 25 84315517; Tel: +86 25 84315517*

[b]*University of Dar es Salaam, P.O. Box 35061, Dar es Salaam, Tanzania*

† Electronic supplementary information (ESI) available. See DOI: 10.1039/c6ra09559c

This journal is © The Royal Society of Chemistry 2016

Published on 27 May 2016. Downloaded by University of Dar es Salaam on 9/18/2018 10:19:08 AM.

Although the effect of steam on catalysts has been reported in some studies,[23–27] basic lithium phosphate (abbreviated as B-Li_3PO_4) catalyst has not yet been studied. In this work, we investigated the effect of steam treatment on basic lithium phosphate catalyst in the propylene oxide rearrangement reaction. The results demonstrated that the product yield of allyl alcohol improved. Moreover, the carbon deposition was suppressed after steam treatment at high temperature. Because the carbon deposition takes place on the acid sites,[28] we considered that the decrease of the amount of Brønsted acid sites resulted in the reduction of carbon deposition. Additionally, the catalytic activity enhancement originates from an increase in synergistic sites resulting from the increase in the number of Lewis acid sites and in the strength of the base sites.

2. Experimental

2.1. Catalyst preparation

Lithium hydroxide monohydrate was dissolved in 100 mL of deionized water at 60 °C in a 500 mL three-necked flask with a stirrer. A solution prepared from sodium phosphate dodecahydrate and water was dropped into the flask with stirring for 3 h. The resulting white precipitate was centrifuged and rinsed with deionized water four times. The precipitate was dried at 120 °C for 12 h and then calcined at 320 °C for 8 h.

For steam treatment, about 1 g of lithium phosphate catalyst thus prepared was further treated at T °C in flowing steam and then maintained at T °C for t h. Thus, steam treated lithium phosphate catalysts were obtained. Here, "ST" means steam treatment. The "t" represents the time of steam treatment in hours and the "T" represents the temperature of the steam treatment.[19] Therefore, a steam treated basic lithium phosphate catalyst at T °C for t h is described as the B-Li_3PO_4 (ST-t h/T °C) catalyst.

2.2. Catalytic activity tests

Catalytic rearrangement reactions were conducted in a fixed-bed reactor. The catalyst (1.0 g, particle diameter of 0.3 to 0.45 mm) was placed in a tube (10 mm diameter) with a thermocouple in contact with the catalyst bed. A mixture of N_2 and vaporized propylene oxide stream was introduced into the reactor. The reaction temperature was controlled at the optimal reaction temperature of 300 °C, and the WHSV (propylene oxide) was 9 h^{-1}.[29] The products were measured by on-line gas chromatography using an Agilent FF-AP capillary column. The product yield of allyl alcohol (AA rate) (kg_{AA} h^{-1} $kg_{cat}{}^{-1}$) was defined as given below:

$$\text{AA rate} = \rho_{PO} \times V_{PO} \times \alpha_{PO} \times S_{AA} \times 60/m \quad (1)$$

where ρ_{PO} is the density of propylene oxide (g cm^{-3}), V_{PO} is the volume of propylene oxide (mL min^{-1}), α_{PO} is the conversation of propylene oxide, S_{AA} is the selectivity of allyl alcohol, and m is the mass of the catalyst (g).

2.3. Catalyst characterization

The Brunauer–Emmett–Teller (BET) surface area was determined by N_2 adsorption–desorption measurements at 77 K (Gold App V-sorb 2008). Powder X-ray diffraction (XRD) was carried out with a general X-ray diffraction instrument (Beijing Purkinjie XD-3, Cu Kα, voltage = 36 kV, electrical current = 30 mA, 2θ = 5 to 80°). The crystallite size was calculated from Scherrer's equation ($D = 0.9\lambda/\beta \cos\theta$, where D is the crystallite size, λ is the wavelength of X-ray radiation (0.15406 for Cu Kα radiation), β is the full length at half-maximum of the (101) peak of the catalyst, and θ is the diffraction angle). Transmission electron microscope (TEM) observations were carried out using a Philips Tecnai 12 instrument. The used catalysts were characterized by thermogravimetric analysis (TG, Mettler-Toledo TGA/SDTA851e) at the rate of 10 °C min^{-1} in nitrogen (99.999%, 30 mL min^{-1}) atmosphere. X-ray photoelectron spectroscopy (XPS) experiments were carried out on a RBD-upgraded PHI-5000C ESCA system (Perkin Elmer) with Mg Kα radiation ($h\nu$ = 1253.6 eV), calibrated by the C 1s peak at 284.6 eV, with an accuracy of 0.1 eV.

Diffuse reflectance-Fourier transform infrared spectroscopy (DRIFTS) was used to investigate the hydroxyl groups of the basic lithium phosphate catalyst under different treatment conditions. Moreover, *in situ* DRIFTS was used to study the selective poisoning of acid sites and the surface acidity of the catalysts. The spectra were recorded on a Nicolet iS10 spectrometer equipped with an iZ10 Auxiliary Module, which consists of a liquid-N_2-cooled high-sensitivity MCT-A detector and a DRIFTS cell (Spectra-Tech) with KBr windows. For the selective poisoning of acid sites, the catalysts adsorbed pyridine at 50 °C and were purged by N_2 for 30 min to remove the gaseous pyridine; then, a background spectrum was recorded. Next, propylene epoxide was admitted into the cell at 50, 100, 200 and 300 °C, and the corresponding spectrum was recorded, respectively. In order to analyse the Lewis acid sites and Brønsted acid sites, the catalysts were characterized by infrared spectroscopy of pyridine adsorption (pyridine-IR). Firstly, a background spectrum was recorded. Then, approximately 50 μL (excess) of pyridine was admitted into the cell at 50 °C; subsequently, the spectra were recorded at 200 and 350 °C, respectively. All spectra were recorded after cooling the sample to 50 °C. For pyridine-IR, the spectra were recorded on a FTIR-Frontier instrument (PE Company) with an *in situ* infrared cell system.

Ammonia temperature-programmed desorption (NH_3-TPD) and carbon dioxide temperature-programmed desorption (CO_2-TPD) experiments were carried out under a flow of He (70 cm^3 min^{-1}) over 100 mg of catalyst. Prior to the TPD experiments, the catalysts were preheated under a flow of He at 350 °C for 1 h, followed by cooling to room temperature under the same He flow. The NH_3 or CO_2 adsorption experiments were conducted under a flow rate of 70 mL min^{-1} at room temperature. Subsequently, the temperature was raised to 500 °C at a heating rate of 10 °C min^{-1}, and the NH_3 or CO_2 desorption profile was obtained.

Published on 27 May 2016. Downloaded by University of Dar es Salaam on 9/18/2018 10:19:08 AM.

3. Results and discussion

3.1. Structural and chemical characterizations

The physical properties of the B-Li_3PO_4 and B-Li_3PO_4 (ST-0.5 h/300 °C) catalysts are listed in Table 1. The BET data of the catalysts demonstrated that there was a gradual increase in surface area from 20 to 23 $m^2\ g^{-1}$ for the B-Li_3PO_4 and B-Li_3PO_4 (ST-0.5 h/300 °C) catalysts. The average pore diameter and the pore volume also increased. The crystallite sizes, which were calculated from the XRD patterns using the Scherrer equation, are also shown in Table 1. It was found that the crystallite size also increased from 32.1 nm of the untreated catalyst to 40.1 nm of the treated catalyst. The larger surface area may provide more adsorptive sites for gas reactants and benefit the mass transfer process.[30] Thus, the steam treatment resulted in high catalytic efficiency for the B-Li_3PO_4 catalyst.

Fig. 1 shows representative TEM images of the untreated B-Li_3PO_4 catalyst and the B-Li_3PO_4 (ST-0.5 h/300 °C) catalyst. It can be seen that B-Li_3PO_4 is a hollow sphere. Although the corresponding TEM images illustrated that there was a slight change at the edge of the B-Li_3PO_4 (ST-0.5 h/300 °C) catalyst, the B-Li_3PO_4 catalyst and the B-Li_3PO_4 (ST-0.5 h/300 °C) catalyst retained their original hollow morphologies. For the steam untreated catalyst, the particle sizes ranged from 0.7 to 1 μm. However, the particle size of the catalyst was about 0.7 μm after steam treatment. It was found that the distribution of particle size became more homogeneous after steam treatment. At the same time, the dispersion became homogeneous after steam treatment, which may be due to the solution-precipitation processes.[31] Fig. S1† shows XRD patterns of the B-Li_3PO_4 catalyst and the B-Li_3PO_4 (ST-*T* °C) catalysts. The patterns did not show any characteristic changes in the structure of the catalysts. The TEM result was consistent with the XRD results. Therefore, the B-Li_3PO_4 catalysts could maintain stable morphology even after steam treatment.

The TG-DTG technique was employed to study the effect of steam treatment on carbon deposition on the B-Li_3PO_4 catalysts.[32] The TG-DTG curves are shown in Fig. 2. It can be seen that the weight loss ratios of the used B-Li_3PO_4 catalyst and the used B-Li_3PO_4 (ST-0.5 h/300 °C) catalyst were 21.5% and 15.1%, respectively. This demonstrated that the carbonaceous species which formed during the propylene oxide rearrangement were significantly suppressed on the B-Li_3PO_4 (ST-0.5 h/300 °C) catalyst compared with the untreated B-Li_3PO_4 catalyst.

There was a distinct decrease in mass in the temperature range from 300 to 500 °C, and the weight loss ratios were 13.6% and 8.4%, respectively. This step may result from the decomposition of hydrocarbons, *i.e.*, carbon deposition. For the untreated catalyst,

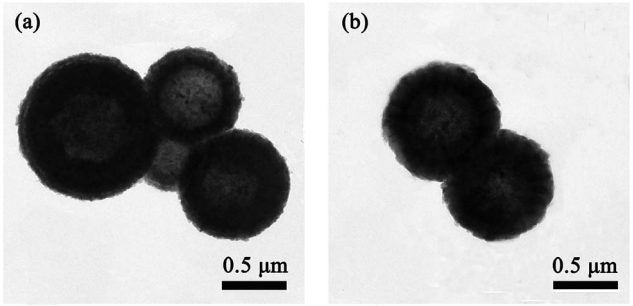


Fig. 1 TEM images of (a) the B-Li_3PO_4 catalyst and (b) the B-Li_3PO_4 (ST-0.5 h/300 °C) catalyst.

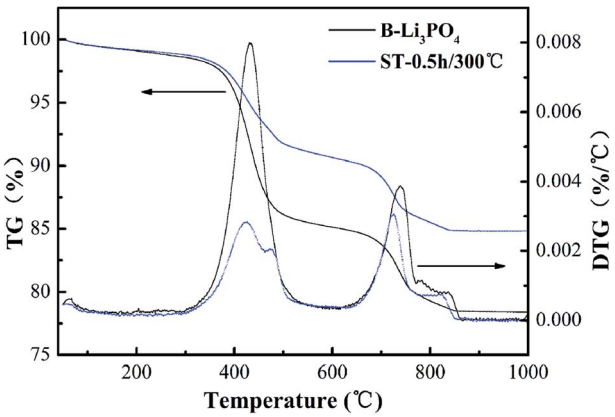


Fig. 2 TG-DTG curves of the B-Li_3PO_4 catalyst and the B-Li_3PO_4 (ST-0.5 h/300 °C) catalyst after being used for 12 h in N_2 atmosphere.

there was a decomposition peak with T_{max} = 420 °C, which corresponds to young coke with low molecular weight or a high H/C.[29] However, for the B-Li_3PO_4 (ST-0.5 h/300 °C) catalyst, there was a main peak at 420 °C and a small, broad peak at 475 °C which corresponds to older coke with a low H/C. Another distinct decrease in mass was observed in the temperature range from 600 to 850 °C, and the weight loss ratios of the catalysts were similar. Therefore, it could be concluded that steam treatment mainly suppressed young coke with low molecular weight or high H/C. This is because the carbon deposition was suppressed after steam treatment; this will be discussed in the following section.

3.2. The effect of steam treatment on the catalytic activity

The catalytic performance results of propylene oxide rearrangement on the B-Li_3PO_4 catalyst and the B-Li_3PO_4 (ST-*t* h/*T* °C)

Table 1 Properties of the B-Li_3PO_4 and the B-Li_3PO_4 (ST-0.5 h/300 °C) catalysts

Catalyst	Surface area[a] ($m^2\ g^{-1}$)	Average pore diameter[a] (nm)	Pore volume[a] ($cm^3\ g^{-1}$)	Crystallite size[b] (nm)
B-Li_3PO_4	20	110.2	0.07	32.1
ST-0.5 h/300 °C	23	148.7	0.11	40.1

[a] Obtained from the BET results. [b] Calculated from the XRD patterns by the Scherrer equation.

 This journal is © The Royal Society of Chemistry 2016

Published on 27 May 2016. Downloaded by University of Dar es Salaam on 9/18/2018 10:19:08 AM.

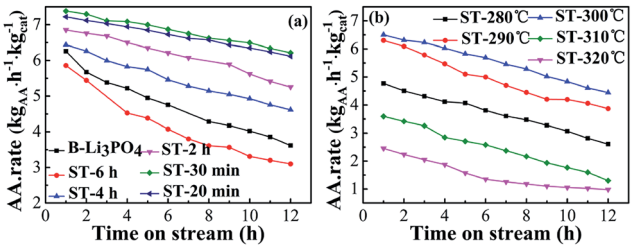


Fig. 3 Production yield of allyl alcohol treated with steam (a) for different times at 300 °C and (b) at different temperatures for 30 minutes after being used for 12 h.

catalysts after being used for 12 h are shown in Fig. 3. It can be seen that the yield of allyl alcohol increased on the steam treated catalyst compared with the untreated B-Li_3PO_4 catalyst.

The effect of the steam treatment time of the B-Li_3PO_4 catalysts on their catalytic performance was also investigated. Fig. 3a demonstrates that the catalytic performance of the B-Li_3PO_4 catalysts was very sensitive to the time of steam treatment. With an increase of the steam treatment time from 20 minutes to 5 hours, all of the B-Li_3PO_4 (ST-*t* h) catalysts exhibited higher activity than the untreated B-Li_3PO_4 catalyst. However, excessive steam treatment, *i.e.*, with longer treatment time (6 h), may lead to a great decrease in the base sites, which is unfavourable to the reaction.

The effect of the steam treatment temperature of the B-Li_3PO_4 catalysts on their catalytic performance is shown in Fig. 3b. This figure demonstrates that the B-Li_3PO_4 catalyst which was treated at 300 °C showed the best catalytic performance. Apparently, among these samples, the B-Li_3PO_4 catalyst which was treated at 300 °C for 30 minutes showed the best performance.

The catalytic performance results of the propylene oxide rearrangement on the untreated B-Li_3PO_4 catalyst and the B-Li_3PO_4 (ST-0.5 h/300 °C) catalyst after being used for 12 h are listed in Table 2. It can be seen that not only did the propylene oxide conversion and the allyl alcohol yield increase on the steam treated catalyst compared with those on the untreated catalyst, but also the selectivity of allyl alcohol increased on the B-Li_3PO_4 (ST-0.5 h/300 °C) catalyst. Among these side products, the selectivity of propionaldehyde and acetone slightly changed. However, the selectivity of isopropyl alcohol and *n*-propyl alcohol decreased on the B-Li_3PO_4 (ST-0.5 h/300 °C) catalyst, in comparison with that of the B-Li_3PO_4 catalyst. Therefore, after steam treatment, the selectivity of allyl alcohol slightly increased on the B-Li_3PO_4 (ST-0.5 h/300 °C) catalyst.

3.3. Discussion of the reaction mechanism

3.3.1. Determination of surface hydroxyl groups (DRIFTS and XPS). DRIFTS and XPS were carried out to investigate the surface hydroxyl groups of the B-Li_3PO_4 catalyst and the B-Li_3PO_4 (ST-0.5 h/300 °C) catalyst, owing to the important function of the surface hydroxyl groups for propylene oxide rearrangement.

The impact of steam on the behaviour of B-Li_3PO_4 catalyst was investigated *via* FTIR spectral techniques. The role of steam may be associated with the surface hydroxyl groups. The FTIR spectra of the fresh B-Li_3PO_4 catalysts treated at different temperatures with steam are shown in Fig. 4. The peaks at

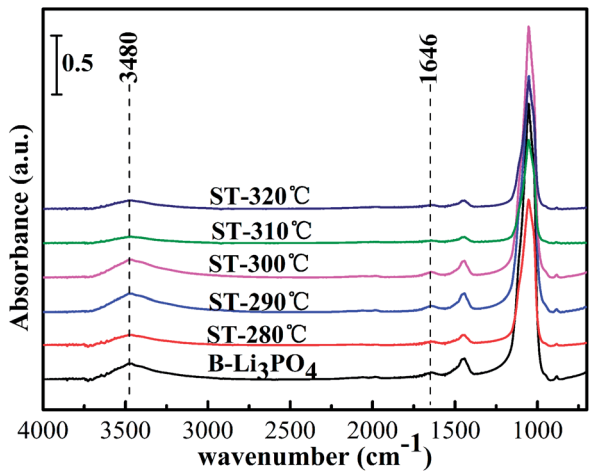


Fig. 4 FTIR spectra of fresh B-Li_3PO_4 catalysts treated with steam at different temperatures.

Table 2 Comparison of catalytic behaviors between the B-Li_3PO_4 and the B-Li_3PO_4 (ST-0.5 h/300 °C) catalysts at different time[a]

			S (%)					
Catalyst	R.T. (h)	Conv (%)	PA	AC	IPA	NPA	AA	AA rate $kg_{AA}\ h^{-1}\ kg_{cat}^{-1}$
B-Li_3PO_4	3	55.5	5.8	6.4	1.3	1.8	84.8	4.7
	6	40.0	5.7	7.0	0.5	1.2	85.6	3.4
	9	36.0	5.5	6.6	0.4	1.1	86.4	2.8
	12	33.5	5.2	6.4	0.4	1.0	87.0	2.9
ST-0.5 h/300 °C	3	70.6	5.4	6.4	0.4	1.0	86.9	6.1
	6	65.7	4.9	5.7	0.4	0.9	88.2	5.8
	9	55.6	6.2	6.8	0.3	0.8	85.9	4.8
	12	54.4	4.7	5.4	0.3	0.8	88.9	4.8

[a] R.T.: reaction time, Conv: conversation, *S*: selectivity, PA: propionaldehyde, AC: acetone, IPA: isopropyl alcohol, NPA: *n*-propyl alcohol, AA: allyl alcohol, AA rate: the yield of allyl alcohol.

Published on 27 May 2016. Downloaded by University of Dar es Salaam on 9/18/2018 10:19:08 AM.

3480 cm^{-1} and 1646 cm^{-1} were ascribed to the O–H stretching and bending vibrations, respectively.[33] The peak of the O–H bending vibration was too weak to easily analyse. However, we could clearly see that the intensity of the peak at 3480 cm^{-1} was different for the catalysts treated at different temperatures. An attempt was made to quantitatively compare the amount of hydroxyl groups. The area ratio of hydroxyl (~3480 cm^{-1}) to PO_4^{3-} (~1100 cm^{-1}) was employed to quantitatively estimate the amount of hydroxyl groups for all the catalysts. The ratio of the untreated catalyst was 0.18, and those of the catalysts treated at 280, 290, 300, 310 and 320 °C were 0.23, 0.24, 0.26, 0.23 and 0.22, respectively. The area ratio of hydroxyl to PO_4^{3-} increased obviously from 0.18 for the untreated catalyst to 0.26 for the treated catalyst at 300 °C. The ratio, *i.e.*, the amount of hydroxyl groups, was in exact accordance with the order of the catalytic activity shown in Fig. 3b. This indicated that the hydroxyl groups promoted the catalytic activity of the B-Li_3PO_4 catalyst. The nature of the hydroxyl groups was further examined by XPS.

Fig. 5 shows typical XPS results together with fitted O1s peaks. Table 3 summarizes the results of the O1s peaks. It can be seen from Fig. 5 that the peaks were asymmetric. Also, the O1s peaks were perfectly fitted to three peaks. For both catalysts, in addition to the lattice oxygen with a binding energy of 529.7 eV, the surface of the catalysts contained hydroxyl groups with a binding energy of 530.6 eV and a minor amount of adsorbed water with a binding energy of 531.7 eV.[34,35]

In order to quantitatively compare the hydroxyl groups, the area ratios of OH to P were calculated (Table 3).[36,37] The ratio of the steam treated catalyst was greater than that of the untreated catalyst. Moreover, the area of the adsorbed water for the steam treated catalyst was also slightly greater than that of the untreated catalyst. The hydroxyl groups preferentially formed when the catalyst was treated with steam. Combining with Fig. 3, it can be seen that the steam treated catalyst with an area ratio of 1.43 had greater activity than the untreated catalyst with an area ratio of 1.04. Therefore, we again verified that the enhancement of catalytic activity was connected with the formation of hydroxyl groups after steam treatment. Because the production of allyl alcohol requires strong base sites as active sites,[17,18] we speculated that the role of the hydroxyl groups was associated with its base sites. NH_3-TPD and CO_2-TPD were employed to further verify this speculation.

3.3.2. Determination of catalyst acidity and basicity (NH_3-TPD, CO_2-TPD, *in situ* FTIR and pyridine-IR). NH_3-TPD is an efficient technique to measure the amount and strength of acids. The peak area of the TPD profile represents the amount of desorbed NH_3, whereas the peak position corresponds to the acid strength of the catalyst. The profiles of the untreated and the steam treated samples are shown in Fig. 6. For the untreated catalyst, the peaks are perfectly fitted to three peaks, which represent three acid centres. In addition to the weak acid centre with T_{max} = 143 °C and the strong acid centre with T_{max} = 321 °C, there was a medium acid centre. After treatment, there were two distinctive ammonia desorption peaks in the profiles. The first peak with T_{max} = 157 °C represented the weak acid sites, and the second peak with T_{max} = 373 °C corresponded to the strong acid sites. We considered that the weak and strong acid sites originated from P=O···H and Li^+, respectively. It could be observed from the peak area that the total acid amount decreased; however, the acid strength of the strong acid sites became stronger after treatment. Because the phosphate ion has covalent character,[38] according to theoretical computations we have performed, lithium bound with oxygen is prone to provide electrons and change into lithium ion after steam treatment. The calculated results using Mulliken population analysis of the charges of the water molecules and their individual atoms before and after steam treatment are shown in Table 4. We found that after water adsorption on Li_3PO_4 (100), the charge of the Li atom increased from 0.96 to 0.98. At the same time, the charge of the O atom increased from −1.25 to −1.18. These results indicated that both the Li and O atoms lost electrons. In addition, we found that the charge of the P atom

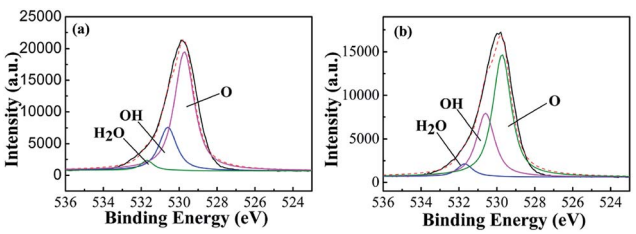


Fig. 5 O 1s XPS profiles of (a) the B-Li_3PO_4 catalyst and (b) the B-Li_3PO_4 (ST-0.5 h/300 °C) catalyst.

Table 3 Chemical compositions (atom%) of the catalysts based on the XPS analyses

	O_{1s}/%					
Catalyst	O	OH	H_2O	P_{2p}/%	Li_{1s}/%	OH/P
B-Li_3PO_4	59.1	19.2	3.2	18.5	<0.1	1.0
ST-0.5 h/300 °C	50.8	26.3	4.5	18.4	<0.1	1.4

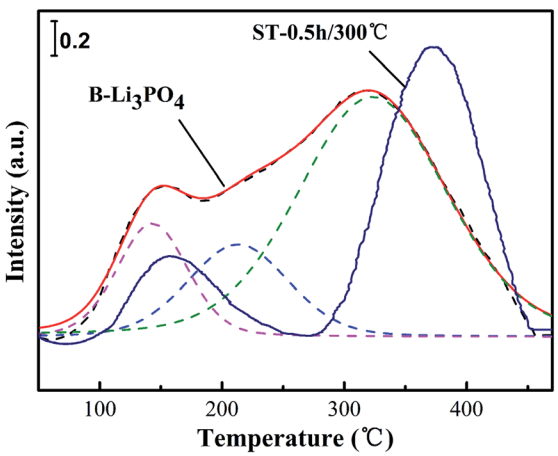


Fig. 6 NH_3-TPD profiles of the B-Li_3PO_4 catalyst fitted with three peaks and of the B-Li_3PO_4 (ST-0.5 h/300 °C) catalyst.

This journal is © The Royal Society of Chemistry 2016

Published on 27 May 2016. Downloaded by University of Dar es Salaam on 9/18/2018 10:19:08 AM.

Table 4 Mulliken charges for a water molecule adsorbed on the Li_3PO_4 (100) surface of the configuration BV

	H_1	H_2	$O(H_2O)$	Li	$O(Li_3PO_4)$	P
Isolated H_2O	0.53	0.53	−1.06			
Li_3PO_4 (100)				0.96	−1.25	2.21
H_2O on Li_3PO_4 (100)	0.47	0.42	−1.04	0.98	−1.18	2.21

retained a value of 2.23. In order to take the balance of the charge into consideration, the Mulliken charges for the water molecule changed from 0.00 to −0.15. These suggested that the water molecule received some electrons from the Li and O atoms. The lithium ion may act as a stronger acid site. Hence, steam treatment could change the nature and distribution of the acid sites. Because the carbon deposition generally takes place on the acid sites,[28] we considered that the decrease of the total acid amount resulted in a reduction of the carbon deposition. This explains why steam treatment can suppress the carbon deposition.

CO_2-TPD was employed to measure the base amount and strength.[39,40] The profiles of the steam untreated and treated catalysts are shown in Fig. 7. There were two carbon dioxide desorption peaks in the profiles. For the steam treated catalyst, the first peak with $T_{max} = 120$ °C represented the weak base sites (P═O) and the second peak with $T_{max} = 320$ °C corresponded to the strong base sites. The strong base sites may originate from hydroxyl groups connected with Li, that is, Li–OH. However, for the steam untreated catalyst, four main desorption peaks were observed at 130 °C, 180 °C, 280 °C and 320 °C, indicating four kinds of base sites on the surface of the catalyst. The peaks at 130 °C and 320 °C can be ascribed to the weak and strong base sites, respectively. The peaks centered at 180 °C and 280 °C can be assigned to the relatively weak base sites and the relatively strong base sites of the catalyst, respectively. In other words, steam treatment changed the distribution of the base sites to form distinct weak and strong base sites. From the changes of the peak locations, it was observed that the strength of the relatively weak base sites weakened slightly and the strength of the relatively strong base sites increased after steam treatment. Therefore, the amount of strong base sites increased significantly, which may result from the formation of Li–OH. Also, the amount of weak base sites decreased, which may be due to the transition from P═O to P–OH. Because strong base sites are favorable to improve the activity of basic catalysts,[41] according to what we have speculated from Fig. 4 and 5, we could conclude that the hydroxyl groups improved the catalytic performance due to the stronger base sites after steam treatment.

In situ FTIR was performed to further determine the active sites of propylene oxide rearrangement,[42] and the results are presented in Fig. 8. After pyridine was adsorbed on the basic lithium phosphate catalyst at 50 °C, an absorption peak at 1454 cm^{-1} attributed to pyridine bound to the Lewis acid sites was observed. Additionally, the FTIR spectra after evacuation of pyridine at different temperatures (Fig. 9) demonstrated that the adsorption of pyridine on the Lewis acid sites was strong and that complete desorption did not occur, even at 350 °C. When propylene oxide was subsequently introduced, it was found that the adsorption peak of pyridine bound to Lewis acid sites decreased significantly and even almost disappeared at 300 °C (optimal reaction temperature), which was a strong indication of the competitive adsorption of propylene oxide and pyridine on the Lewis acid sites. That is to say, propylene oxide was prone to adsorb on the Lewis acid sites. In other words, the Lewis acid sites were the active sites for propylene oxide rearrangement on the basic lithium phosphate catalyst. Hence, the improvement of the catalytic activity may originate from the increase of the amount of Lewis acid sites after steam treatment.

To verify the speculation that the amount of Lewis acid sites increased after steam treatment, the changes in the FTIR spectra after adsorption of pyridine on the catalysts[43,44] before and after steam treatment are compared in Fig. 9. The amount of pyridine evacuated at 200 °C represented the total amount of acid sites. Also, the amount of pyridine evacuated at 350 °C represented the medium and strong acid sites. The base sites of

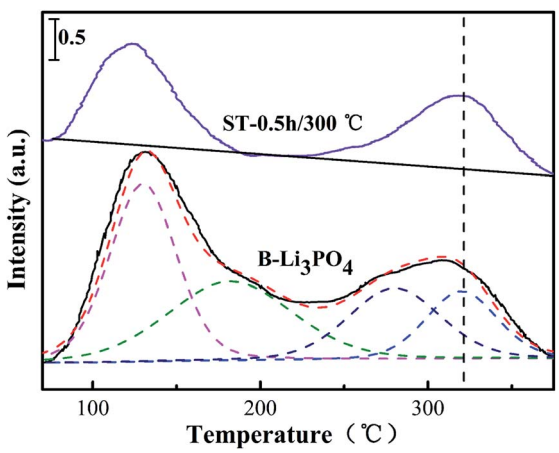


Fig. 7 CO_2-TPD profiles of the B-Li_3PO_4 catalyst fitted with four peaks and of the B-Li_3PO_4 (ST-0.5 h/300 °C) catalyst.

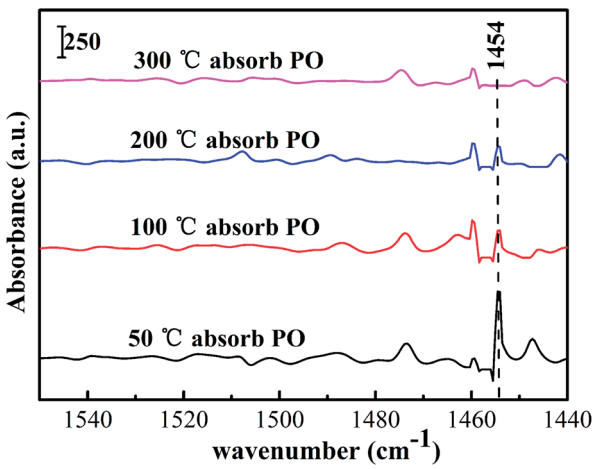


Fig. 8 *In situ* FTIR spectra of propylene oxide rearrangement on the fresh B-Li_3PO_4 catalysts.

Published on 27 May 2016. Downloaded by University of Dar es Salaam on 9/18/2018 10:19:08 AM.

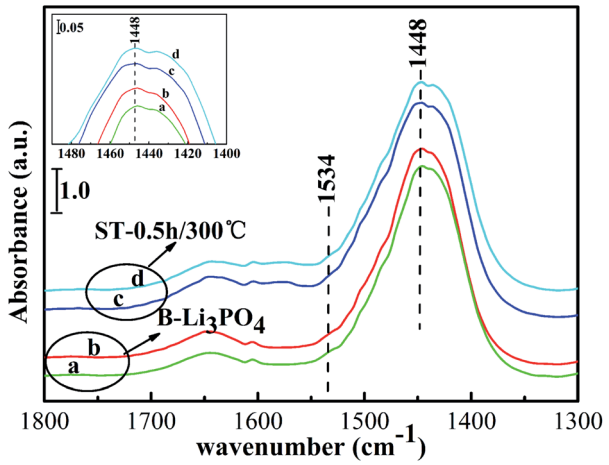


Fig. 9 FTIR spectra of pyridine adsorption on the B-Li_3PO_4 catalyst and the B-Li_3PO_4 (ST-0.5 h/300 °C) catalyst evacuated at (a and c) 200 °C and (b and d) 350 °C, respectively.

lithium phosphate catalyst are prone to absorb carbon dioxide from the air. Because the peak of the C–O stretching vibration of CO_3^{2-} appeared at 1400 to 1500 cm^{-1} in the spectrum,[45] the broad peak around 1450 cm^{-1} assigned to CO_3^{2-} can be seen (Fig. 9). The peaks of pyridine coordinated on Brønsted acid sites and Lewis acid sites should appear around 1540 cm^{-1} and 1450 cm^{-1}, respectively.[46–48] Therefore, the peaks of pyridine coordinated on Brønsted acid sites and Lewis acid sites will be overlapped by the peak of CO_3^{2-}. For both catalysts, a slight change could still be seen in the peaks at 1534 cm^{-1} and 1448 cm^{-1}. It could be speculated that this may result from the presence of Brønsted acid sites and Lewis acid sites.

To quantify the acid sites of the untreated and the steam treated catalysts, the integral area of the bands at 1534 cm^{-1} (Brønsted acid sites) and 1448 cm^{-1} (Lewis acid sites) were used. The concentrations of Brønsted and Lewis acid sites was calculated by the following formula[49] and are listed in Table 5.

$$C_L = 1.42\mathrm{IA(L)}R^2/W \quad (2)$$

$$C_B = 1.88\mathrm{IA(B)}R^2/W \quad (3)$$

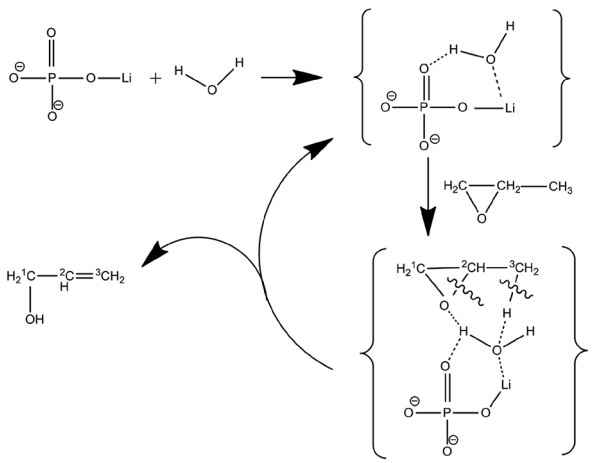
where C_B is the concentration of pyridine on the Brønsted acid sites (mmol g^{-1} catalyst), C_L is the concentration of pyridine on the Lewis acid sites (mmol g^{-1} catalyst), IA(B, L) is the integrated absorbance of the B or L band (cm^{-1}), R is the radius of the catalyst disk (cm), and W is the weight of the disk (mg).

In Fig. 9, curves a and c represent the pyridine evacuation of the untreated catalyst and the steam treated catalyst at 200 °C, respectively. The results show that the concentration of total Lewis acid sites increased from 0.029 for the untreated catalyst to 0.031 for the steam treated catalyst. Curves b and d represent the pyridine evacuation of the untreated catalyst and the steam treated catalyst at 350 °C, respectively. It can be seen that the concentration of medium and strong Lewis acid sites increased from 0.014 for the untreated catalyst to 0.020 for the steam treated catalyst. Because of the limited amount of Brønsted acid sites, the peak at 1534 cm^{-1} (Brønsted acid sites) was not obvious. The amount of Brønsted acid sites could not be determined quantitatively. Because the NH_3-TPD results showed that the total amount of acid sites decreased, according to the increase of the amount of Lewis acid sites, the concentration of Brønsted acid sites must decrease. Numerous papers have proved that the Brønsted acid sites promote the formation of carbon deposition.[20,21] Hence, it could be concluded that the decrease of Brønsted acid sites resulted in the reduction of carbon deposition. The activity enhancement originated from the increase in the amount of Lewis acid sites. Because the phosphate ion has covalent character,[38] according to our theoretical computations, lithium bound with oxygen was prone to provide electrons and change into lithium ion after steam treatment. Hence, the lithium ions acted as Lewis acid sites. Due to the increase of lithium ion, the amount of Lewis acid sites increased. In conclusion, according to CO_2-TPD, we can conclude that the stronger base sites attributed to hydroxyl groups were beneficial to improve the activity of basic catalysts after steam treatment. Based on the FTIR spectra of pyridine adsorption (Fig. 8 and 9), due to the increase of the amount of Lewis acid sites, which are the active sites for propylene oxide rearrangement on basic lithium phosphate catalyst, the catalytic activity was enhanced. Hence, we propose that the activity enhancement came from the increase of synergistic sites resulting from the increase in the amount of Lewis acid sites and in the strength of the base sites.

Table 5 Concentration of Lewis acid sites determined by pyridine adsorption at different evacuation temperatures

Catalyst	200 °C (mmol g^{-1})	350 °C (mmol g^{-1})
B-Li_3PO_4	0.029	0.014
ST-0.5 h/300 °C	0.031	0.020

For the reaction mechanism of propylene oxide rearrangement, Yasuaki Okamoto *et al.*[41] have proposed a mechanism. For the reaction mechanism after steam treatment, a new reaction mechanism has been proposed in the presence of basic lithium phosphate catalyst. The possible mechanism is shown as follows.



This journal is © The Royal Society of Chemistry 2016

Published on 27 May 2016. Downloaded by University of Dar es Salaam on 9/18/2018 10:19:08 AM.

After H_2O molecule is absorbed on the lithium phosphate catalyst, the hydrogen atom and the oxygen atom of the H_2O molecule can combine with the oxygen of P=O and with lithium, respectively, and an intermediate is formed. Furthermore, the formation of Li–OH increases the strength of the base sites of the catalyst. When propylene oxide is absorbed on the intermediate, the oxygen of H_2O combines with the α-hydrogen of propylene oxide. The bond strength of O–H in H_2O weakens and the bond breaks. At the same time, the bond of ^{2}C–O breaks and ^{1}C–OH is formed. The electron density of the two other carbon atoms becomes negative and a $^2C{=}^3C$ bond is formed. Thus, allyl alcohol is formed and the intermediate returns to the original state.

4. Conclusions

A simple steam treatment method was developed to improve the catalytic performance and enhance the coke resistance of basic lithium phosphate catalyst for propylene oxide rearrangement. The basic lithium phosphate catalyst had the highest activity when the catalyst was treated with steam at 300 °C for 30 minutes. TEM micrographs showed that there was a slight change at the edge of the B-Li_3PO_4 (ST-0.5 h/300 °C) catalyst. From TG-DTG analysis, it could be seen that steam treatment could suppress young coke with low molecular weight or with high H/C. NH_3-TPD demonstrated that the suppression might result from a decrease in the amount of Brønsted acid sites. According to CO_2-TPD, we could conclude that the stronger base sites attributed to the hydroxyl groups were beneficial to improve the activity of the basic catalyst after steam treatment. Based on the FTIR spectra of pyridine adsorption (Fig. 8 and 9), due to the increase of the amount of Lewis acid sites which were the active sites for propylene oxide rearrangement on basic lithium phosphate catalyst, the catalytic activity was enhanced. Hence, we propose that the activity enhancement originates from the increase of synergistic sites resulting from the increase in the amount of Lewis acid sites and in the strength of the base sites.

Acknowledgements

The authors are grateful to the Natural Science Foundation (No. 21276127 and 51106076) and the Priority Academic Program Development of Jiangsu Higher Education Institutions (PAPD).

Notes and references

1 M. W. C. Robinson, K. S. Pillinger, I. Mabbett, D. A. Timms and A. E. Graham, *Tetrahedron*, 2010, **66**, 8377–8382.
2 E. Ertürk, M. Göllü and A. S. Demir, *Tetrahedron*, 2010, **66**, 2373–2377.
3 O. de la Torre, M. Renz and A. Corma, *Appl. Catal., A*, 2010, **380**, 165–171.
4 H.-Q. Xiao, X.-Z. Shu, K.-G. Ji, C.-Z. Qi and Y.-M. Liang, *Catal. Commun.*, 2009, **10**, 1824–1827.
5 D. P. Serrano, R. van Grieken, J. A. Melero, A. García and C. Vargas, *J. Mol. Catal. A: Chem.*, 2010, **318**, 68–74.
6 J. Jitputti, B. Kitiyanan, P. Rangsunvigit, K. Bunyakiat, L. Attanatho and P. Jenvanitpanjakul, *Chem. Eng. J.*, 2006, **116**, 61–66.
7 K. Maruoka, T. Ooi and H. Yamamoto, *J. Am. Chem. Soc.*, 1989, **111**, 6431–6432.
8 K. Ishihara, N. Hanaki and H. Yamamoto, *Synlett*, 1995, **1995**, 721–722.
9 K. A. Bhatia, K. J. Eash, N. M. Leonard, M. C. Oswald and R. S. Mohan, *Tetrahedron Lett.*, 2001, **42**, 8129–8132.
10 I. Karamé, M. L. Tommasino and M. Lemaire, *Tetrahedron Lett.*, 2003, **44**, 7687–7689.
11 A. Procopio, R. Dalpozzo, A. D. Nino, M. Nardi, G. Sindona and A. Tagarelli, *ChemInform*, 2005, **36**, 2633–2635.
12 S. Kohji, K. Taketoshi, N. Shin-Ichiro and T. Toshikatsu, *J. Am. Chem. Soc.*, 2004, **126**, 9554–9555.
13 K. Suda, S. Nakajima, Y. Satoh and T. Takanami, *Chem. Commun.*, 2009, 1255–1257, DOI: 10.1039/b820948k.
14 Z. Pakulski, M. Koprowski and K. Michał Pietrusiewicz, *Tetrahedron*, 2003, **59**, 8219–8226.
15 P. Dinér, *Tetrahedron: Asymmetry*, 2010, **21**, 2733–2739.
16 K. Arata and K. Tanabe, *Catal. Rev.*, 1983, **25**, 365–420.
17 C. Raptis, H. Garcia and M. Stratakis, *Angew. Chem., Int. Ed. Engl.*, 2009, **48**, 3133–3136.
18 T. Imanaka, Y. Okamoto and S. Teranishi, *Bull. Chem. Soc. Jpn.*, 1972, **45**, 1353–1357.
19 M. Usman and W. M. A. W. Daud, *RSC Adv.*, 2015, **5**, 21945–21972.
20 P. M. Boorman, K. Chong, R. A. Kydd, J. M. Lewis, P. M. Boorman, K. Chong, R. A. Kydd and J. M. Lewis, *J. Catal.*, 1991, **128**(2), 537–550.
21 J. Fei, Z. Hou, B. Zhu, H. Lou and X. Zheng, *Appl. Catal., A*, 2006, **304**, 49–54.
22 H. Wang, L. Su, J. Zhuang, D. Tan, Y. Xu and X. Bao, *J. Phys. Chem. B*, 2003, **107**, 12964–12972.
23 I. H. Son, S. J. Lee, A. Soon, H.-S. Roh and H. Lee, *Appl. Catal., B*, 2013, **134–135**, 103–109.
24 Z. Nawaz and F. Wei, *J. Ind. Eng. Chem.*, 2010, **16**, 774–784.
25 A. Yamaguchi, D. Jin, T. Ikeda, K. Sato, N. Hiyoshi, T. Hanaoka, F. Mizukami and M. Shirai, *Catal. Commun.*, 2015, **69**, 20–24.
26 P. Duprez, M. Hadj-Aissa and J. Barbier, *Stud. Surf. Sci. Catal.*, 1991, **68**, 111–118.
27 X. Yan, M. Ke, Z. Song, Q. Jiang and P. Yu, *RSC Adv.*, 2016, **6**, 14799–14808.
28 T. Horiuchi, K. Sakuma, T. Fukui, Y. Kubo, T. Osaki and T. Mori, *Appl. Catal., A*, 1996, **144**, 111–120.
29 L. Jiang, H. Li, Y. Wang, W. Ma and Q. Zhong, *Catal. Commun.*, 2015, **64**, 22–26.
30 Y. Zhang, F. Liu and J. Zhang, *J. Phys. Chem. C*, 2010, **114**, 16929–16936.
31 Z. Pei, J. Chen and X. Zhang, *Nanosci. Nanotechnol. Lett.*, 2012, **4**, 457–459.
32 L. Yao, J. Shi and C. Hu, *RSC Adv.*, 2015, **5**, 90168–90177.
33 W. Niu, D. Ren, Y. Han, Y. Wu and X. Gou, *J. Alloys Compd.*, 2012, **543**, 159–166.
34 J. T. Kloprogge, L. V. Duong, B. J. Wood and R. L. Frost, *J. Colloid Interface Sci.*, 2006, **296**, 572–576.

Published on 27 May 2016. Downloaded by University of Dar es Salaam on 9/18/2018 10:19:08 AM.

35 H. R. Ong, M. M. Rahman Khan, A. Yousuf, N. A. Hussain and C. K. Cheng, *RSC Adv.*, 2015, **5**, 100362–100368.
36 B. Erdem, R. A. Hunsicker, G. W. Simmons, E. D. Sudol, V. L. Dimonie and M. S. El-Aasser, *Langmuir*, 2001, **17**, 2664–2669.
37 Q. Zhang, H. Liu, X. Zhan, F. Chen, J. Yan and H. Tang, *RSC Adv.*, 2015, **5**, 77508–77517.
38 J. B. Moffat, *Catal. Rev.: Sci. Eng.*, 1978, **18**(2), 199–258.
39 X. Jiao, H. Li, L. Li, F. Xiao, N. Zhao and W. Wei, *RSC Adv.*, 2014, **4**, 47012–47020.
40 C. Zhong, X. Guo, D. Mao, S. Wang, G. Wu and G. Lu, *RSC Adv.*, 2015, **5**, 52958–52965.
41 Y. Okamoto, T. Imanaka and S. Teranishi, *Bull. Chem. Soc. Jpn.*, 1973, **46**, 4–8.
42 Q. Dai, L.-L. Yin, S. Bai, W. Wang, X. Wang, X.-Q. Gong and G. Lu, *Appl. Catal., B*, 2016, **182**, 598–610.
43 M. N. Alaya and M. A. Rabah, *J. Alloys Compd.*, 2013, **575**, 285–291.
44 S. Lai, D. Meng, W. Zhan, Y. Guo, Y. Guo, Z. Zhang and G. Lu, *RSC Adv.*, 2015, **5**, 90235–90244.
45 C. Rey, B. Collins, T. Goehl, I. R. Dickson and M. J. Glimcher, *Calcif. Tissue Int.*, 1989, **45**, 157–164.
46 X. Wang, J. C. Yu, P. Liu, X. Wang, W. Su and X. Fu, *J. Photochem. Photobiol., A*, 2006, **179**, 339–347.
47 T. Takeguchi, K.-i. Yanagisawa, T. Inui and M. Inoue, *Appl. Catal., A*, 2000, **192**, 201–209.
48 F. Hemmann, I. Agirrezabal-Telleria, C. Jaeger and E. Kemnitz, *RSC Adv.*, 2015, **5**, 89659–89668.
49 C. A. Emeis, *J. Catal.*, 1993, **141**, 347–354.

This journal is © The Royal Society of Chemistry 2016